

# PCCP

Accepted Manuscript



This is an *Accepted Manuscript*, which has been through the Royal Society of Chemistry peer review process and has been accepted for publication.

*Accepted Manuscripts* are published online shortly after acceptance, before technical editing, formatting and proof reading. Using this free service, authors can make their results available to the community, in citable form, before we publish the edited article. We will replace this *Accepted Manuscript* with the edited and formatted *Advance Article* as soon as it is available.

You can find more information about *Accepted Manuscripts* in the [Information for Authors](#).

Please note that technical editing may introduce minor changes to the text and/or graphics, which may alter content. The journal's standard [Terms & Conditions](#) and the [Ethical guidelines](#) still apply. In no event shall the Royal Society of Chemistry be held responsible for any errors or omissions in this *Accepted Manuscript* or any consequences arising from the use of any information it contains.

# Optical properties of a conjugated-polymer-sensitised solar cell: the effect of interfacial structure

Daniel W. Drumm,<sup>\*a,b</sup> A. Bilic,<sup>c</sup> Y. Tachibana<sup>d</sup>, A. Miller<sup>c</sup>, and S. P. Russo<sup>a</sup>

Received 24th October 2014, Accepted Xth XXXXXXXXX 20XX

First published on the web Xth XXXXXXXXX 200X

DOI: 10.1039/b000000x

Dye-sensitised solar cells (DSSCs) have sparked considerable interest over two decades. Recently, a method of polymer-wire sensitisation was demonstrated; the polymer is suggested to form a hole transport pathway (wire) following initial charge separation. We predict the optical properties of this polymer in various interfacial configurations, including the effects of chain length and attachment to {100} or {101} TiO<sub>2</sub> facets. Contrary to most DSSCs, the {100} facet model best describes the experimental spectrum, predicting a relative thickness of 5.7±0.2 μm, although {101} attachment, if implemented, may improve collection efficiency. Long chains are optimal, and stable attachment sites show minimal differences to absorbance in the major solar emission (visible) band. Combinations of {100}, {101}, and pseudo-bulk TiO<sub>2</sub> models in three-parameter fits to experiment confirm the relative importance of the {100} facet.

## 1 Introduction

Since O'Regan and Grätzel revolutionised the dye sensitised solar cell (DSSC)<sup>1</sup>, there has been strong, consistent interest in exploiting it as a clean renewable energy source<sup>2</sup>. Raising cell efficiency and lowering production costs constitute major foci<sup>2-4</sup>. Recent efforts to improve efficiency include increasing the light harvesting of the solar spectrum<sup>5</sup>, sensitizer regeneration efficiency<sup>6</sup>, charge transport rates<sup>7</sup>, and minimising charge recombination loss mechanisms<sup>8</sup>. In terms of minimising loss, one avenue towards improving DSSC performance is increasing charge separation efficiency at semiconductor/dye interfaces. This is governed by two competing processes: charge separation of the exciton at the interface including electron transfer into the conduction band, and charge recombination which is a loss mechanism<sup>2</sup>.

Conjugated polymer sensitisation is one of the most attractive strategies to achieve high light-harvesting efficiency and sufficient charge-separation. Conjugated polymers display relatively high extinction coefficients over a wide range of wavelengths. Their band gaps can be tunable<sup>9</sup>, allowing control of the driving force of charge transfer reactions. Inten-

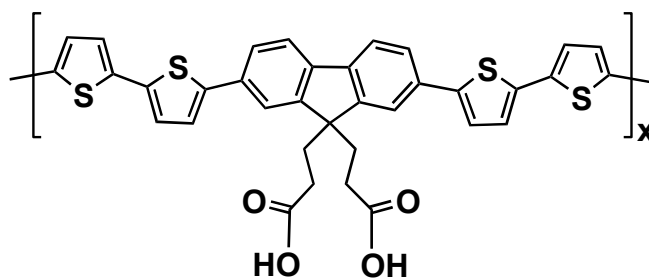


Fig. 1 Poly(2,7-bis(bithiophene)fluorene-9,9-dipropionic acid).

sive efforts have been focussed upon polymer structure modification to optimise these parameters<sup>2</sup>; solar energy conversion efficiencies as high as 3.8% have been reported<sup>10</sup>. Recently a conjugated-polymer wire on nanoporous metal-oxide system was developed<sup>11</sup>, showing retardation of the charge recombination rate by a factor of 50-70. The polymer is believed to donate an electron to the TiO<sub>2</sub> substrate, and then conduct the hole (act as a wire), effecting good charge separation. In this paper, we determine how oligo/polymer chain length, attachment point, and substrate facet affect the optical properties of the system described in Ref. 11. We use *ab initio* density functional theory (DFT)<sup>12,13</sup>, modelling the wire (Fig. 1) before forming cells with titania substrates, mimicking the experimental situation. DFT has previously been successful in describing the optical properties of several systems<sup>14-17</sup>, and has been applied to smaller DSSC cluster models in combination with time-dependent DFT<sup>18-21</sup> (TD-DFT).

<sup>a</sup> Theoretical Chemical and Quantum Physics, School of Applied Sciences, RMIT University, Melbourne VIC 3001, Australia. E-mail: daniel.drumm@rmit.edu.au

<sup>b</sup> Now at the Australian Research Council Centre of Excellence for Nanoscale BioPhotonics, School of Applied Sciences, RMIT University, Melbourne VIC 3001, Australia.

<sup>c</sup> CSIRO Computational Informatics, Private Bag 33, Clayton South VIC 3169, Australia.

<sup>d</sup> School of Aerospace, Mechanical and Manufacturing Engineering, RMIT University, Bundoora VIC 3083, Australia.

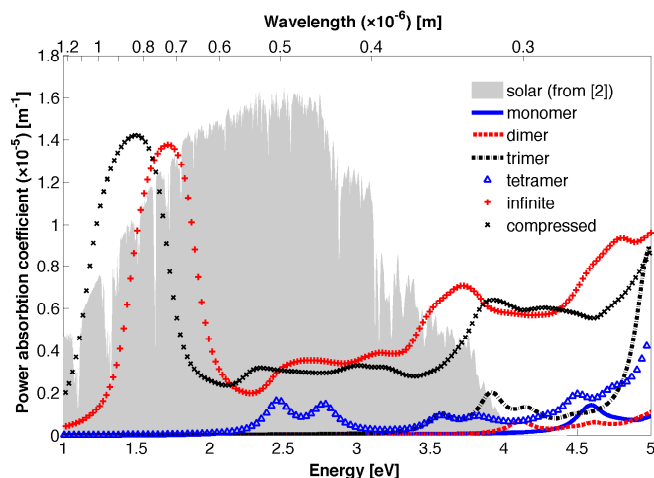


**Fig. 2** Power absorption coefficient of monomer–tetramer, infinite, and compressed wires, with solar irradiation spectrum (arb. scale).

## 2 Results and Discussion

### 2.1 Oligomer properties

Figure 2 displays the power absorption (also called attenuation) coefficients of the dye monomer and various oligomers (which for full models shall be scaled by the sample thickness to give the actual absorbance), alongside the solar irradiance spectrum<sup>2</sup>. The coefficients are significant in the visible regime (1.5–3.2 eV). The monomer's absorbance edge is near 4.3 eV (tangent to the first peak at its half-maximum value, extrapolated to the frequency axis), which is in the ultraviolet spectrum. Polymerisation leads to a reduction in the absorbance edge frequency, with further polymerisation leading to greater reductions into the visible regime. The natural extension of this concept is to a polymer of infinite chain length, which has been constructed from the monomer via rotations to align the molecule with the  $x$  axis of the simulation, where periodic boundary conditions have been imposed upon the linking bond as shown in Fig. 1. This infinite molecule was further relaxed, including the cell length, to allow for optimal positioning. Its coefficients are also shown in Fig. 2, with the absorbance edge (and major peak) falling around 1.3 (1.7) eV, well into the infrared spectrum. Clearly, longer wires are better-matched to the solar irradiation; their extension to the infinite limit carries this process too far, although the infinite wire still absorbs throughout the visible spectrum.

### 2.2 Addition of {101} TiO<sub>2</sub> slab

Since the 23.8 Å monomer is adsorbed onto 15–20 nm diameter TiO<sub>2</sub> nanoparticles before polymerisation<sup>22</sup>, the TiO<sub>2</sub> was approximated as a few-monolayer slab. The most stable form

of TiO<sub>2</sub> nanoparticles (hydrogenated, diameter <23 nm) is the anatase phase<sup>23</sup>, whose {101} facets are stable and common to the manufacturing process used by the suppliers of Ref. 11<sup>22,24–26</sup> and to theory models describing other dyes<sup>18–21</sup>.

A 12-atom bulk anatase TiO<sub>2</sub> unit cell was therefore optimised, giving lattice parameters ( $a$ ,  $b$ ,  $c$ ) of 3.7967, 9.5211, and 3.7967 Å respectively. This unit cell was used to develop a (6×2) {101} slab comprised of three (O–Ti–O) 22.73Å × 20.45Å layers, providing the closest supercell length (in  $x$ ) to the monomer (23.8Å), and other dimensions (in  $y$  and  $z$ ) incorporating at least 10 Å of vacuum about the molecule to separate it from its periodically replicated neighbours (and neighbouring slab). Due to computational intractability, longer slabs sufficient to contain dimer or larger oligomer units were not modelled, although the additional flexibility in such models might be desirable. The infinite wire (67 atoms) was then uniformly compressed along its length slightly to fit with the slab supercell, the terminal H atoms on the COOH groups were removed, and the wire randomly placed upon the slab (aligned along the  $x$  axis). 24 additional models were developed by applying shifts parallel to the slab (along  $x$  and  $y$ ) corresponding to multiples of 1/5 of the unit slab lengths, resulting in a 5×5 uniform grid of attachment points across the unit slab. These 25 complete models were re-optimised keeping the bottom (O–Ti–O) layer pinned in bulk positions while the upper two layers and wire were relaxed to simulate the nanoparticle surface. To control for any compression effects, another model of the lone infinite, periodic polymer was constructed with the reduced cell length.

Figure 2 also shows the compressed wire's absorption. The compression has little effect other than a slight redshift below 3 eV. As the absorbance edge is still well into the infra-red, and the compressed wire is relaxed further in the polymer-slab models, the compression is of negligible concern here.

The slab-wire combinations were relaxed (apart from the pinned layer mentioned earlier), resulting in structures still subject to considerable forces. To obtain the best placement(s) of the polymer on the slab, the primitive slab surface was divided using a 5×5 grid with the initial position at (0,0) and others ranging up to (4,4); these coordinates will be used to label the models henceforth. Rotations of the molecule relative to the slab were precluded by the periodic boundary conditions of the simulation. New models were created using the shifted polymer position coordinates, and relaxed. Absorbances were predicated upon a nominal 6 μm sample thickness in line with the 6–7 μm thickness detailed experimentally<sup>27</sup>.

The absorbances of the 24 lowest-energy {101} configurations (ranging over 0.3 eV, with 130 eV to the last model), were quite similar from 1.7 eV upwards. From 1 to 1.7 eV, four models showed a smaller, blueshifted peak (1.7 eV from 1.4). Figure 3 shows a comparison of six representative spectra with the solar irradiation spectrum.

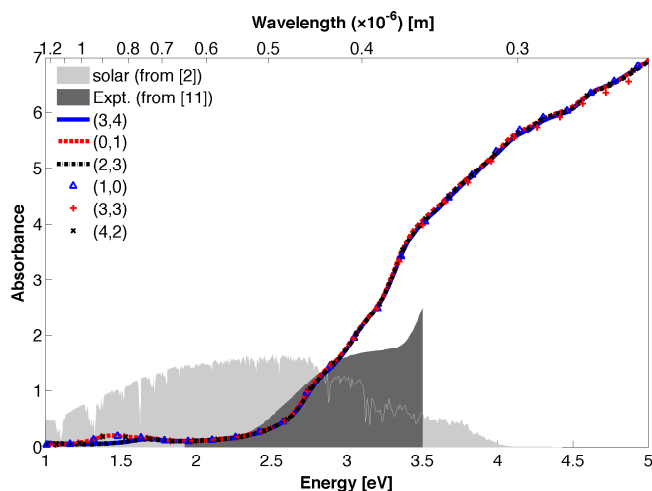


**Fig. 3** Absorbances of the six lowest-energy  $\{101\}$  models, solar irradiance spectrum (arb. scale), and experimental absorbance graphically estimated from Ref. 11 (actual scale).

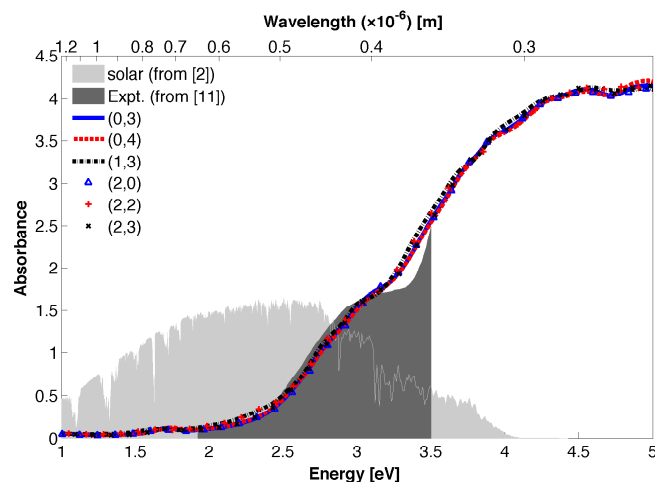


**Fig. 4** Absorbances of the six lowest-energy  $\{100\}$  models, solar irradiance spectrum (arb. scale), and experimental absorbance graphically estimated from Ref. 11 (actual scale).

### 2.3 Polymer on $\{100\}$ -facet models

The match between the calculated  $\{101\}$ -facet absorbances and the experimental spectrum, while reasonable from 1.9 to 2.7 eV, is not good from 2.7 to 3.5 eV. One possibility is that this particular dye prefers to attach to the  $\text{TiO}_2$  nanoparticles on an alternate face. According to an *ab initio* model, the  $\{100\}$  facets of anatase nanoparticles are only slightly higher in energy than the  $\{101\}$  facets<sup>23</sup>. This is also supported by experimental observations<sup>28</sup>, sometimes depending on the growth conditions<sup>29</sup>, and it is also recognised that even when the  $\{101\}$  facets are prevalent, a considerable fraction of the remaining surface area is  $\{100\}$ <sup>25</sup>. Thus, a repeat of the simulations on a new  $\{100\}$  slab were undertaken.

The  $\{100\}$  slab, comprised of five neutral ( $6 \times 2$ )  $22.92 \text{ \AA} \times 20.63 \text{ \AA}$  monolayers of  $\text{TiO}_2$ , was surface-relaxed holding the lowest two monolayers pinned in bulk positions. The slab dimensions necessitated a similar compression of the wire monomer to fit the periodic boundary conditions along its length (in  $x$ ). Again, the wire was added at a random position plus 24 other positions on a uniform  $5 \times 5$  grid across the unit slab for a total of 25  $\{100\}$ -slab-wire models.

The six lowest-energy  $\{100\}$  configurations ranged over 1.2 eV total energy, with 2 eV to the next-lowest. They also had the lowest forces, at 32–116 meV/ $\text{\AA}$ . Their absorbances are shown in Fig. 4, where they are prominent from 2 eV upwards. Strikingly, the absorbance of each conformation is almost identical down to 1 eV (well outside the visible region of the spectrum, and irrelevant to this application). Small differences in methods of stable attachment only result in changes to the low-frequency end of the spectrum.

Comparison to Ref. 11 (via Fig. 4) shows extraordinary

agreement between the calculated absorbance for a 6  $\mu\text{m}$  thickness of the proposed model and the experimental absorbance (graphically estimated from Ref. 11) over most of the overlapping spectral region, with good correspondence for the higher-energy region from 3.2–3.5 eV. Inspection of Figs. 3 and 4 supports  $\{100\}$  facet model attachment over  $\{101\}$ .

Whilst DFT is known to sometimes underestimate band gaps<sup>30,31</sup>, optical properties are calculated directly using the full band structure and will be subject to the same error, allowing us to extract at least qualitative information. The agreement with experiment inspires confidence that this calculation does not suffer drastically from band gap error.

### 2.4 Fitting the experimental spectrum

Exploring the concept of a preferred attachment facet begs the question: to what extent does either family of model reflect reality? Here, 15–20 nm diameter nanocrystals of  $\text{TiO}_2$  are treated as slabs of up to 2.2 nm in-plane as required to isolate the attached dye polymer from periodic images of itself. The reality is the experimental situation: a 6–7  $\mu\text{m}$  layer of aggregated, randomly oriented  $\text{TiO}_2$  nanocrystals with various facets, coated with polymers in an unknown arrangement (see Fig. 1b of Ref. 11). To first order, the likelihood of a particular facet type having a certain orientation can be considered uniform over all solid angles. For this reason, the tensor contraction chosen (see Sec. 3) to derive the scalar dielectric function is the isotropic average. The models above make a further (unrealistic) assumption: that only one facet type is present.

Secondly, some vacuum space will necessarily be about the nanocrystals, due to hard-shell packing considerations, and larger voids (pores) are also possible given the randomness of

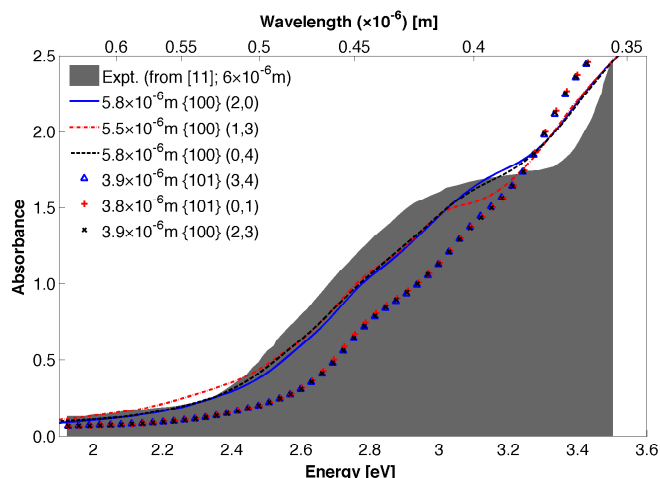


Fig. 5 Absorbances of best-thickness fits to Ref. 11.

the material. Both theoretical results ( $\{101\}$  and  $\{100\}$ ) overestimate the experiment for part of the high-energy spectrum. A first approximation to their suitability to represent the experimental data is then to allow the effective thickness of the complete layer to vary, via the least-squares approximation:

$$\min \left\{ \sum_i [a_{\text{facet}} \times A_{\text{facet}}(i) - A_{\text{exp.,est.}}(i)]^2 \right\}, \quad (1)$$

where  $i$  ranges across the energy values of the estimates to the experimental absorbance (values of  $A_{\text{facet}}$  are linearly interpolated to these energies),  $A_{\text{exp.,est.}}$ ,  $a_{\text{facet}}$  scales the absorbance  $A_{\text{facet}}$ , and  $\{\text{facet}\}$  is replaced by  $\{100\}$  or  $\{101\}$  as required.

Figure 5 shows the experimental results of Ref. 11 along with the best three least-squares fits (Eq. 1) of model thicknesses for each facet model's absorbance in the common region (1.9–3.5 eV). By inspection, the  $\{100\}$ -facet models best fit the spectrum with a consistent effective thickness of  $5.7 \pm 0.2 \mu\text{m}$  (or 97% of the nominal  $6 \mu\text{m}$  thickness). The  $\{101\}$ -facet models give less visually satisfying (although consistent) fits at  $3.9 \pm 0.3 \mu\text{m}$  effective thickness. The sums of squares (SS) for the models bear this qualitative comparison out, with the  $\{100\}$  models' SS 4–7 times smaller than the  $\{101\}$  models' SS. Again, this is further evidence in favour of attachment via the non-standard  $\{100\}$  facet.

There are two logical physical interpretations of  $a_{\text{facet}}$ . First, the layer could genuinely be narrower. However, despite the agreement between the  $\{100\}$ -facet result and the reported experimental thickness, this view is unphysical as the material in question is not a bulk crystal. It is unlikely that the nanocrystals stack perfectly, facet against facet, and in any case room is not allowed for the polymer to coat the nanocrystals. Further, the overall structure would have a more common (therefore not uniformly random) orientation in contravention of the as-

sumption behind taking the isotropic average. Second, the difference could be due to vacuum space between the nanocrystals. In this case, the  $\{100\}$  model implies that the experimental sample contains between 3 and 17% vacuum depending upon whether its actual thickness is nearest 6 or  $7 \mu\text{m}$ .

A more reasonable approximation can be made by allowing the two facet models to mix. Fitting a two-parameter equation,

$$\min \left\{ \sum_i [a_{\{100\}} \times A_{\{100\}}(i) + a_{\{101\}} \times A_{\{101\}}(i) - A_{\text{exp.,est.}}(i)]^2 \right\}, \quad (2)$$

allows better flexibility. Here, since both calculated absorbances reference the same nominal  $6 \mu\text{m}$  thickness, their scaling coefficients are directly comparable and represent the equivalent fraction of a new  $6 \mu\text{m}$  hybrid material. This equation was fit to every combination of the 6  $\{100\}$  and 24  $\{101\}$  models. The total contribution ( $a_{\{100\}} + a_{\{101\}}$ ) ranged over 92–97%, with a maximum 7% contribution from the  $\{101\}$  facet. The minimum SS reported was 1.46 (as compared to the 1.49 for the one-parameter  $\{100\}$  fit). The evidence suggests that the polymer preferentially attaches to the  $\{100\}$  facet.

Of course, 15–20 nm nanocrystals are not comprised entirely of 5 surface  $\{100\}$  or  $\{101\}$  monolayers alone. They also include some rarer facets, such as  $\{001\}$ , and the bulk-like  $\text{TiO}_2$  in the centre. There is thus some merit to including the pseudo-bulk substrate structure in the modelling.

On the dual bases that the relaxed  $\{100\}$   $\text{TiO}_2$  positions differ subtly from those of bulk, and that the  $\{100\}$  surface relaxation would be evident over a large proportion of the nanocrystal surface, a three-parameter model was constructed thus:

$$\min \left\{ \sum_i [a_{\{100\}} \times A_{\{100\}}(i) + a_{\{101\}} \times A_{\{101\}}(i) + a_{\{\text{slab}\}} \times A_{\{\text{slab}\}}(i) - A_{\text{exp.,est.}}(i)]^2 \right\}, \quad (3)$$

and fit to the same 144 model combinations. Again, comparisons between the scaling coefficients give deeper understanding of the relative contributions of each material type to the overall absorbance. Here, the total contribution is more tightly bounded at 84–86% of nominal. This consists of 75–84% “pseudo-bulk slab”, followed by 0–10%  $\{100\}$ -attached polymer, and 0–0.09%  $\{101\}$ -attached polymer.

Analysis of the SS shows similar results, with the range over all 144 combinations being 1.345–1.346, 10% less than the minimum value for the one-parameter model and 8% less than the best two-parameter model. The relative importance of the  $\{100\}$  facet over the  $\{101\}$  is preserved. This model also provides the most realistic quantities of vacuum. At 14–28%, depending on the actual thickness ranging from 6– $7 \mu\text{m}$ , scope for considerable space between nanocrystals is maintained.

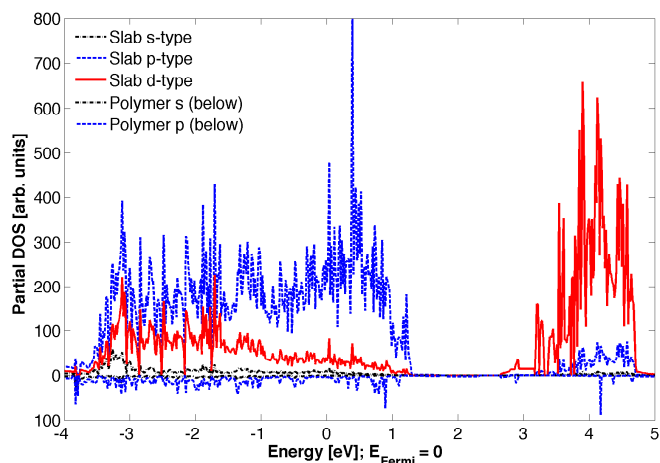


**Fig. 6** Partial electronic densities of states of the (2,0) slab (above) and polymer (below). Note that these densities are *not* spin-resolved.

Although it is tempting to claim that the polymer preferentially attaches to anatase {100} facets, several other considerations must be dealt with first. The effect of rotating the polymer on either surface has not been established, due to the use of periodic boundary conditions and the size of the supercells used. Similarly, size-related effects of the relative amount of TiO<sub>2</sub> compared to dye polymer in the model have not been explored (due to computational intractability). Additionally, if the optical properties as calculated are directly comparable, then attaching this polymer to {101} facets could result in better absorbance above 2.7 eV. However, the result does beg the question: should other dyes previously modelled on {101} facets of TiO<sub>2</sub> be investigated on {100} as well?

## 2.5 Electronic density of states

The major consequence of dye sensitisation is the easy capture of the exciton's electron into the TiO<sub>2</sub> conduction band, separating it from the hole which remains trapped in the dye (and in this case, is funnelled along the polymerised wire to the cathode). For this to occur, excitons must be created with energies exceeding that of the TiO<sub>2</sub> conduction band(s) into which the electron is expected to transfer. Accordingly, shown in Fig. 6 is the partial electronic density of states (pDOS) of a TiO<sub>2</sub> {100} slab, alongside the pDOS of the attached dye. As the slab has been relaxed to better represent the surface of a nanoparticle, it is expected that some surface states will manifest in the band gap, which indeed is less than the bulk anatase value of 3.2 eV. Slab conduction states are available below the first major feature in the unoccupied pDOS of the situated polymer, and hence charge transfer and separation via TiO<sub>2</sub> conduction can occur after excitation within the polymer.

## 3 Theoretical Methods

Vienna *ab initio* simulation package (VASP)<sup>32</sup> was employed for all calculations, using plane-augmented wave pseudopotentials<sup>33,34</sup>, PBE exchange-correlation functional in the generalised-gradient approximation<sup>35</sup>, plane-wave cutoff energy of 530 eV, and 2×2×2 Monkhorst-Pack<sup>36</sup> *k*-point mesh, unless otherwise specified. These parameters match or exceed those used successfully in other carbon-based systems<sup>37,38</sup>.

The monomer used by Ref. 11 was constructed and preliminarily relaxed via molecular mechanics in AVOGADRO<sup>39</sup> (using a steepest-descent strategy with the MMFF94 force field<sup>40</sup>, at least 500 steps, converging to 1 meV) duplicated, triplicated *etc.*, as required, with appropriate removal of terminal H atoms to construct the dimer, trimer and tetramer, and re-relaxed. The resulting oligomers were readied for DFT by surrounding with at least 10 Å of vacuum space in all directions (except for the infinite case which had zero vacuum about a monomer unit backbone, or in *x*), and were then reoptimised using VASP.

Geometry relaxations proceeded in the following way: first, bulk anatase was fully relaxed; second, the relevant crystalline surface facet was cut and re-relaxed holding the in-plane lattice parameters and lowest two monolayers fixed to adequately represent the surface behaviour of anatase nanoparticles; third, the polymer was placed on the surface aligned along the *x* axis in one of 25 positions regularly spaced on a 5×5 grid across the primitive slab cell - the polymer and non-bulk slab layers were re-relaxed as per step 2.

Geometries were relaxed until the total energy converged below 2 meV. Final structures were subjected to high-accuracy electronic energy minimisation calculations using the Blöchl interpolated tetrahedron smearing method<sup>33</sup>. Properties were calculated using the subsequently acquired wavefunctions.

Optical properties in the form of the complex dielectric tensor function were calculated via linear-response theory<sup>14</sup> and the independent-particle approximation from the DFT models, due to the computational intractability of performing higher-accuracy (GW approximation or TD-DFT) calculations on such large supercells. This is transformed via:

$$\langle \epsilon_{ij}(\omega) \rangle = \frac{1}{3} \text{Tr}[\epsilon_{ij}(\omega)] = \frac{1}{3} \epsilon_{ii}(\omega) = \epsilon(\omega) \quad (4)$$

to the isotropically averaged complex scalar dielectric function, thence via standard transformations<sup>41</sup> to the power absorption coefficient, and to absorbance by multiplication with a nominal thickness in line with experiment. Increasing the *k*-point mesh to 4×4×4 had negligible effect on the monomer spectrum, simply enhancing values from 6 to 8 eV which are irrelevant in the context of the solar spectrum; the standard 2×2×2 *k*-point mesh described above was therefore used for all calculations of the dielectric tensor.

## 4 Conclusions

We have modelled the polymer wire demonstrated in Ref. 11 to sensitise solar cells, both in isolation and on {101} and {100} slabs representative of the TiO<sub>2</sub> substrate used in experiment. The length of the polymer drastically affects its absorbance properties, with increasing chain length accompanying a decrease in the absorbance edge energy (or increase in its wavelength). Models show remarkable agreement with experimental absorbance below 2.7 eV, and those on {100} facets agree well throughout. One-parameter fits of model structures reinforce the conjecture that the experimental spectrum is best explained by polymer attachment via the {100} facet, where a relative thickness of  $5.7 \pm 0.2 \mu\text{m}$  is predicted (compared to 6–7  $\mu\text{m}$  experimentally). Extension to three parameters also involving pseudo-bulk TiO<sub>2</sub> and polymer on {101} facets concur regarding the relative importance of the facets, begging the question of whether dyes previously modelled solely on {101} facets should be revisited. The three-parameter model also allows for 14–28% of the experimental structure to consist of vacuum between nanoparticles in line with the porous nature of the substrate. We have found multiple stable attachment points of the polymer to both substrate facets; these have similar properties, indicating that this particular system is robust against inhomogeneities in the monomer adsorption onto the TiO<sub>2</sub> nanoparticles: experimentalists need not attempt to overly optimise the placement of the monomer on the surface prior to polymerisation.

AB thanks the CSIRO for support through the Julius Career Award. This research was undertaken on the NCI National Facility in Canberra, Australia, which is supported by the Australian Commonwealth Government.

## References

- 1 B. O'Regan and M. Grätzel, *Nature*, 1991, **353**, 737.
- 2 A. Hagfeldt, G. Boschloo, L. Sun, L. Klöö and H. Pettersson, *Chemical Reviews*, 2010, **110**, 6595.
- 3 J.-L. Brédas, J. Norton, J. Cornil and V. Coropceanu, *Accounts of Chemical Research*, 2009, **42**, 1691.
- 4 P. Heremans, D. Cheyns and B. Rand, *Accounts of Chemical Research*, 2009, **42**(11), 1740.
- 5 S. Balasingam, M. Lee, M. Kang and Y. Jun, *Chemical Communications*, 2013, **49**, 1471.
- 6 F. Li, J. Jennings and Q. Wang, *ACS Nano*, 2013, **7**(9), 8233.
- 7 P. Docampo, S. Guldin, U. Steiner and H. Snaith, *The Journal of Physical Chemistry Letters*, 2013, **4**(5), 698.
- 8 J. Gonzalez-Vazquez, G. Oskam and J. Anta, *The Journal of Physical Chemistry C*, 2012, **116**(43), 22687.
- 9 Z. Fang, A. Eshbaugh and K. Schanze, *Journal of the American Chemical Society*, 2011, **133**, 3063.
- 10 K. Akitsu, T. Kubo, S. Uchida, H. Segawa, N. Otani, M. Tomura, T. Tamura and M. Matsumura, *Japanese Journal of Applied Physics*, 2012, **51**, 10NE04.
- 11 Y. Tachibana, S. Makuta, Y. Otsuka, J. Terao, S. Tsuda, N. Kambe, S. Seki and S. Kuwabata, *Chemical Communications*, 2009, **29**, 4360.
- 12 P. Hohenberg and W. Kohn, *Physical Review*, 1964, **136**(3B), B864–B871.
- 13 W. Kohn and L. Sham, *Physical Review*, 1965, **137**(6A), A1697–A1705.
- 14 M. Gajdos, K. Hummer, G. Kresse, J. Furthmüller and F. Bechstedt, *Physical Review B*, 2006, **73**, 045112.
- 15 F. Hossain, M. Doherty, H. Wilson and L. Hollenberg, *Physics Review Letters*, 2008, **101**, 226403.
- 16 R. Bondi, S. Lee and G. Hwang, *Physical Review B*, 2010, **82**, 115214.
- 17 N. Mirzadeh, D. Drumm, J. Wagler, S. Russo and S. Bhargava, *Dalton Transactions*, 2013, **42**, 12883.
- 18 F. D. Angelis, A. Tilocca and A. Selloni, *Journal of the American Chemical Society*, 2004, **126**, 15024.
- 19 F. D. Angelis, S. Fantacci, A. Selloni, M. Nazeeruddin and M. Grätzel, *Journal of the American Chemical Society*, 2007, **129**, 14156.
- 20 F. D. Angelis, S. Fantacci, A. Selloni, M. Nazeeruddin and M. Grätzel, *The Journal of Physical Chemistry C*, 2010, **114**, 6054.
- 21 F. D. Angelis, S. Fantacci, E. Mosconi, M. Nazeeruddin and M. Grätzel, *The Journal of Physical Chemistry C*, 2011, **115**, 8825.
- 22 Private communications with the authors of [11].
- 23 A. Barnard and P. Zapol, *Physical Review B*, 2004, **70**, 235403.
- 24 J. Martens, R. Prins, H. Zandbergen and D. Koningsberger, *The Journal of Physical Chemistry*, 1988, **92**, 1903.
- 25 V. Shklover, M.-K. Nazeeruddin, S. Zakeeruddin, C. Barbe, A. Kay, T. Haiback, W. Steurer, R. Hermann, H.-U. Nissen and M. Grätzel, *Chemistry of Materials*, 1997, **9**, 430.
- 26 C. Barbé, F. Arendse, P. Comte, M. Jirousek, F. Lenzmann, V. Shklover and M. Grätzel, *Journal of the American Ceramic Society*, 1997, **80**(12), 3157.
- 27 Y. Tachibana, S. Makuta, Y. Otsuka, J. Terao, S. Tsuda, N. Kambe, S. Seki and S. Kuwabata, *Chemical Communications*, 2009, **29**, Supp. Mat. 1–16.
- 28 G. Spoto, C. Morterra, L. Marchese, L. Orto and A. Zecchina, *Vacuum*, 1990, **41**(1–3), 37.
- 29 S. Burnside, V. Shklover, C. Barbé, P. Comte, F. Arendse, K. Brooks and M. Grätzel, *Chemistry of Materials*, 1998, **10**, 2419.
- 30 A. Zunger, J. Perdew and G. Oliver, *Solid State Communications*, 1980, **34**, 933–936.
- 31 J. Perdew and A. Zunger, *Physical Review B*, 1981, **23**, 5048–5079.
- 32 G. Kresse and J. Furthmüller, *Physical Review B*, 1996, **54**(16), 11169–11186.
- 33 P. Blöchl, O. Jepsen and O. Andersen, *Physical Review B*, 1994, **49**(23), 16223–16233.
- 34 G. Kresse and D. Joubert, *Physical Review B*, 1999, **59**(3), 1758–1775.
- 35 J. Perdew, K. Burke and M. Ernzerhof, *Physical Review Letters*, 1996, **77**(18), 3865–3868.
- 36 H. Monkhurst and J. Pack, *Physical Review B*, 1976, **13**(12), 5188–5192.
- 37 D. Drumm, M. Per, S. Russo and L. Hollenberg, *Physical Review B*, 2010, **82**(5), 054102.
- 38 S. Bhargava, K. Kitadai, T. Masashi, D. Drumm, S. Russo, V.-W. Yam, K.-M. Lee, J. Wagler, and N. Mirzadeh, *Dalton Transactions*, 2012, **41**(16), 4789–4798.
- 39 M. Hanwell, D. Curtis, D. Lonie, T. Vandermeersch, E. Zurek and G. Hutchison, *Journal of Cheminformatics*, 2012, **4**, 17.
- 40 T. Halgren, *Journal of Computational Chemistry*, 1996, **17**(5-6), 490–519.
- 41 *Handbook of Optics, vol. II: Devices, Measurements, & Properties, 2nd Ed.*, ed. M. Bass, E. V. Stryland, D. Williams and W. Wolfe, McGraw-Hill, 1995.